

# Search for the critical point of strongly interacting matter

## ( Intermittency analysis by NA61/SHINE at CERN SPS )

Haradhan Adhikary for the NA61/SHINE collaboration\*

<sup>1</sup>Jan Kochanowski University, Kielce, Poland

**Abstract.** The existence and location of the QCD critical point is an object of both experimental and theoretical studies. The comprehensive data collected by NA61/SHINE during a two-dimensional scan in beam momentum (13A-150A GeV/c) and system size ( $p+p$ ,  $p+\text{Pb}$ , Be+Be, Ar+Sc, Xe+La, Pb+Pb) allows for a systematic search for the critical point – a search for a non-monotonic dependence of various correlation and fluctuation observables on collision energy and size of colliding nuclei. In particular, fluctuations of particle number in transverse momentum space are studied. They are quantified by measuring the scaled factorial moments of multiplicity distribution.

## 1 Introduction

In this proceeding, experimental results on scaled factorial moments of proton and negatively charged hadron multiplicity distribution in central  $^{208}\text{Pb} + \text{Pb}$  collisions at 13A GeV/c, 30A GeV/c, and  $^{40}\text{Ar} + ^{45}\text{Sc}$  collisions at 13A-150A GeV/c are presented. The measurements were performed by the multi-purpose NA61/SHINE [1] experiment at the CERN Super Proton Synchrotron (SPS). As part of the strong interactions program, the NA61/SHINE studies properties of the onset of deconfinement and searches for the critical point of the strongly interacting matter. Within this program, a two-dimensional scan of collision energy and the size of colliding nuclei was performed [2]. The reported results concern the search for the critical point (CP).

## 2 The NA61/SHINE detector

The NA61/SHINE detector is a large-acceptance hadron spectrometer situated in the North Area H2 beam-line of the CERN SPS [1]. The main components of the detection system are four large-volume Time Projection Chambers (TPCs). This setup allows for precise momentum reconstruction and identification of charged particles. The high-resolution forward hadron calorimeter, the Projectile Spectator Detector (PSD), is used to determine the collision's centrality by measuring the energy of projectile spectators, i.e. non-interacting projectile nucleons.

---

\*e-mail: haradhan.adhikary@cern.ch

### 3 Particle identification

Based on the ionization energy loss ( $dE/dx$ ) in TPCs (Fig. 1) charged particles with different momenta are identified as protons or negatively charged hadrons. As an example of proton selection, the  $dE/dx$  distribution for positive particles is shown in Fig. 1 and the selected region is marked with the red line. On average about 60% of all protons are selected for the analysis. Kaons contaminate this sample by less than 4%.

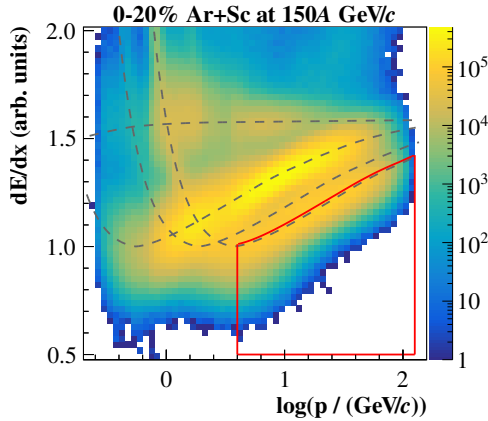


**Figure 1.** Energy loss vs total momentum of positively charged particles measured with the NA61/SHINE Time Projection Chambers (TPCs) in central  $^{40}\text{Ar} + ^{45}\text{Sc}$  collisions at 150A GeV/c. Dashed lines picture the nominal Bethe-Bloch values for protons, kaons, pions and electrons. The cut to select proton candidates is marked with a red line.

A similar procedure was used to select negatively charged hadrons ( $h^-$ ) by removing electrons using  $dE/dx$  cut.

## 4 The critical point search methodology

The goal of the analysis is to search for the critical point of the strongly interacting matter by measuring the scaled factorial moments for mid-rapidity particles using cumulative variables of transverse momenta (section: 4.2) and statistically independent points (section: 4.3).

### 4.1 Critical point and intermittency in heavy-ion collisions

A second-order phase transition leads to the divergence of the correlation length ( $\xi$ ). The infinite system becomes scale-invariant with the particle correlation function having the power-law form, which appears as intermittent behavior of particle multiplicity fluctuations [3]. The intermittent multiplicity fluctuations [4] were discussed as the signal of CP by Satz [5], Antoniou et al. [6] and Bialas, Hwa [7]. This initiated experimental studies of the structure of the phase transition region via analyses of particle multiplicity fluctuations using scaled factorial moments (SFMs) [8]. Later, additional measures of fluctuations were also proposed as probes of the critical behavior [9, 10].

The NA61/SHINE experiment has performed a systematic scan of collision energy and system size. The new measurements may answer the question about the nature of the transition

region and, in particular, whether the critical point of strongly interacting matter exists and where it is located. The scaled factorial moments  $F_r(\delta)$  [4] of order  $r$  are defined as

$$F_r(\delta) = \frac{\left\langle \frac{1}{M} \sum_{i=1}^M N_i(N_i - 1) \dots (N_i - r + 1) \right\rangle}{\left\langle \frac{1}{M} \sum_{i=1}^M N_i \right\rangle^r}, \quad (1)$$

where  $\delta (= \frac{\Delta}{M^{1/D}})$  is the size of each of the  $M$  subdivision intervals of the selected interval  $\Delta$  (two-dimensional bins in the transverse-momentum plane),  $N_i$  is the particle multiplicity in a given interval, and angle brackets denote averaging over the analysed events. If the system at freeze-out is close to the CP, then the system is a simple fractal and  $F_r(\delta)$  follows a power-law dependence:

$$F_r(\delta) = F_r(\Delta) \cdot (\Delta/\delta)^{D \cdot \phi_r}. \quad (2)$$

Moreover, the exponent (intermittency index)  $\phi_r$  obeys the relation:

$$\phi_r = (r - 1)/D \cdot d_r, \quad (3)$$

where  $D$  denotes the dimensionality of the system and the anomalous fractal dimension  $d_r$  is independent of  $r$  [7]. Such behaviour is the analogue of critical opalescence in conventional matter [11].

The QCD-inspired considerations [12, 13] suggest that the critical behaviour can be observed by measuring the fluctuations of the number of protons based on the assumption that the critical fluctuations are transferred to the net-baryon density; the net-baryon density may therefore serve as an order parameter of the phase transition [13–19]. Thus, such fluctuations are expected to be present in the net-proton number and the proton and anti-proton numbers separately [20]. For protons,  $\phi_2 = 5/6$  [11] is expected.

## 4.2 Cumulative transformation

SFMs are sensitive to the shape of the single-particle distribution. The momentum distribution is generally non-uniform and this dependence may bias the signal of critical fluctuations. To remove this dependence one can use cumulative variables [21]. At the same time, it was verified [22] that the transformation preserves the critical behaviour given by Eq. 2. By construction, particle density in the cumulative variables is uniformly distributed. For one-dimensional single-particle distribution in  $x$ , the cumulative variable is

$$Q_x = \int_a^x \rho(x) dx \Big/ \int_a^b \rho(x) dx,$$

where  $a$  and  $b$  are lower and upper limits of the variable  $x$ . For a two-dimensional distribution  $\rho(x, y)$  and a given  $x$  the transformation reads

$$Q_y(x) = \int_a^y \rho(x, y) dy \Big/ \int_a^b \rho(x, y) dy.$$

The distribution of  $Q_x$  and  $Q_y$  is a uniform from 0 to 1 (Fig. 2).

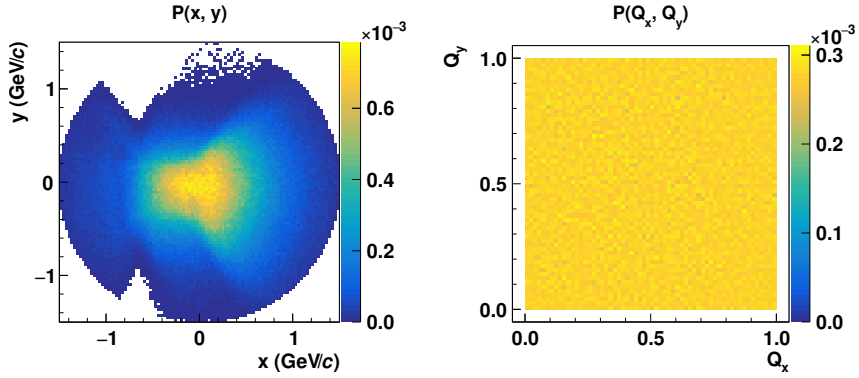


**Figure 2.** Example of the effect of the cumulative transformation of transverse momentum components,  $p_x$  and  $p_y$  (denoted as  $x$  and  $y$ ), selected for proton intermittency analysis of the NA61/SHINE  $^{40}\text{Ar} + ^{45}\text{Sc}$  at 150A GeV/c data. Distribution before (*left*) and after (*right*) the cumulative transformation is presented.

### 4.3 Statistically-independent data points

The intermittency analysis gives the dependence of scaled factorial moments on the number of subdivisions of transverse-momentum or cumulative transverse-momentum space. Here statistically independent data subsets were used to obtain results for each subdivision number. In this case, the results for different subdivision numbers are statistically uncorrelated. Thus the full relevant information needed to interpret the results (the central value and variance) is easy to present graphically and use in the statistical tests. However, the procedure decreases the number of events used to calculate each data point.

## 5 Intermittency analysis results

This section presents the results on scaled factorial moments (Eq. 1) of selected particles ( $p$  or  $h^-$ ) produced by strong and electromagnetic processes in central (0-10%)  $^{208}\text{Pb} + \text{Pb}$  at 13A GeV/c, central (0-10%)  $^{208}\text{Pb} + \text{Pb}$  at 30A GeV/c and central (0-10%)  $^{40}\text{Ar} + ^{45}\text{Sc}$  collisions at 13A-75A GeV/c and central (0-20%)  $^{40}\text{Ar} + ^{45}\text{Sc}$  at 150A GeV/c collisions. The results are shown as a function of the number of subdivisions of cumulative transverse-momentum space – the so-called intermittency analysis. The independent data sets are used for subdivision. The typical acceptance for intermittency analysis is given in [23].

### 5.1 Results for protons in central Pb+Pb collisions

Figures 3 present the dependence of the second-scaled factorial moment for central (0-10%)  $^{208}\text{Pb} + \text{Pb}$  at 13A GeV/c and central (0-10%)  $^{208}\text{Pb} + \text{Pb}$  at 30A GeV/c collisions. The experimental results do not show any significant dependence on  $M$ . There is no indication of the critical fluctuations for selected protons.

### 5.2 Results for protons in central Ar+Sc collisions

Figures 4 present the dependence of the second-scaled factorial moment for central (0-10%)  $^{40}\text{Ar} + ^{45}\text{Sc}$  at 13A-75A GeV/c and central (0-20%)  $^{40}\text{Ar} + ^{45}\text{Sc}$  at 150A GeV/c collisions, The experimental results do not show any significant dependence on  $M$ . There is no indication of the critical fluctuations for selected protons.

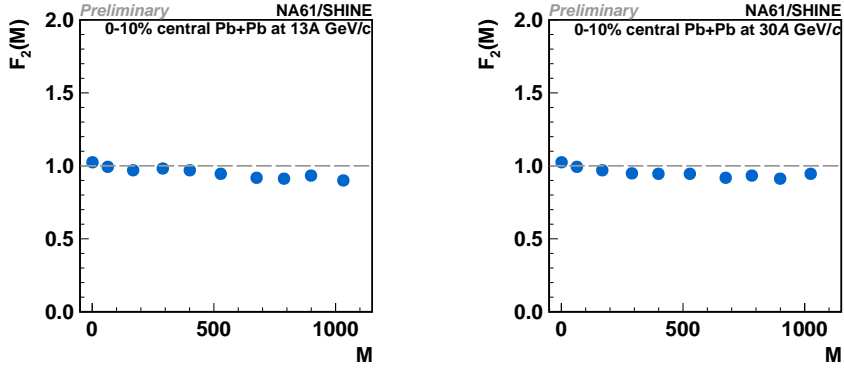


**Figure 3.** The dependence of the second scaled factorial moment of proton multiplicity distribution on the number of subdivisions in cumulative transverse-momentum space  $M$  for  $1 \leq M \leq 32^2$  [22] for central (0-10%)  $^{208}\text{Pb} + \text{Pb}$  at 13A GeV/c (*left*), central (0-10%)  $^{208}\text{Pb} + \text{Pb}$  at 30A GeV/c collisions (*right*). Only statistical uncertainties are indicated.

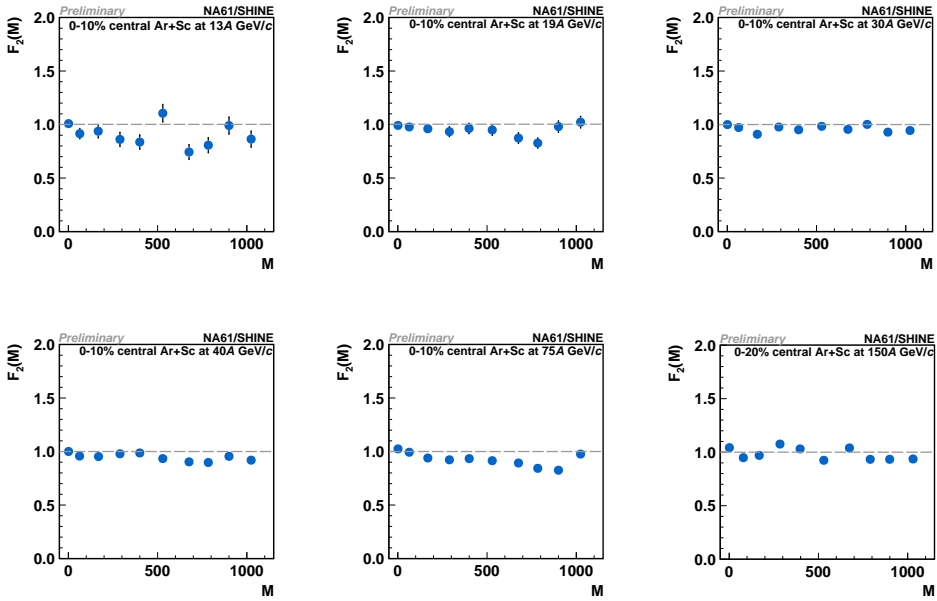


**Figure 4.** The dependence of the second scaled factorial moment of proton multiplicity distribution on the number of subdivisions in cumulative transverse-momentum space  $M$  for  $1 \leq M \leq 32^2$  for central (0-10%)  $^{40}\text{Ar} + ^{45}\text{Sc}$  at 13A-75A GeV/c and central (0-20%)  $^{40}\text{Ar} + ^{45}\text{Sc}$  at 150A GeV/c collisions (from *left top* to *bottom right*). Only statistical uncertainties are indicated.

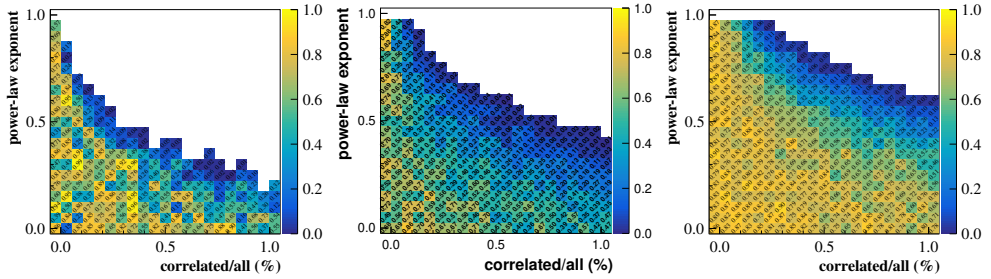


**Figure 5.** Exclusion plot, the p-values, for the Power-law Model parameters – the fraction of correlated protons and the power-law exponent. The white areas correspond to p-values less than 1%. The exclusion plot for  $^{208}\text{Pb} + \text{Pb}$  at 13A GeV/c,  $^{208}\text{Pb} + \text{Pb}$  at 30A GeV/c and  $^{40}\text{Ar} + ^{45}\text{Sc}$  at 150A GeV/c are shown from *left to right*. Exclusion plots for other data sets are expected soon.

### 5.3 Exclusion plots

This section presents exclusion plots for the parameters of the Power-law Model [24] for a comparison of the experimental proton intermittency analysis results of central (0-10%)  $^{208}\text{Pb} + \text{Pb}$  at 13A, central (0-10%)  $^{208}\text{Pb} + \text{Pb}$  at 30A GeV/c and central (0-20%)  $^{40}\text{Ar} + ^{45}\text{Sc}$  at 150A GeV/c collisions.

The model assumes that uncorrelated and correlated protons are produced with an equal to the measured single particle transverse momentum and multiplicity distribution. The model has two controllable parameters:

- (i) fraction of correlated particles
- (ii) power-law exponent of the two-particle correlation function:

$$\rho(|\Delta\vec{p}_T|) \sim |\Delta\vec{p}_T|^{-\phi_2}$$

Many high statistics data sets are produced using the model. Each data set has a different fraction of correlated particles (varying from 0 to 4%) and a different power-law exponent (varying from 0.00 to 0.95).

Next, all generated data sets have been analyzed the same way as the experimental data. Obtained  $F_2(M)$  results have been compared with the corresponding experimental results and  $\chi^2$  and a p-value were calculated. Figure 5 shows obtained p-values as a function of the fraction of correlated protons and the power-law exponent. White areas correspond to a p-value of less than 1% and may be considered excluded.

### 5.4 Results for negatively charged hadrons in central Pb+Pb collisions

Figures 6 present the dependence of the scaled factorial moments of multiplicity distribution of negatively charged hadrons on the number of subdivisions in cumulative transverse momentum space for central (0-10%)  $^{208}\text{Pb} + \text{Pb}$  at 30A GeV/c collisions. For high event multiplicity of negatively charged hadrons, it is possible to calculate scaled factorial moments up to fourth-order moment (Eq. 2). The experimental results do not show any significant dependence on  $M$ . There is no indication of the critical fluctuations for selected negatively charged hadrons.

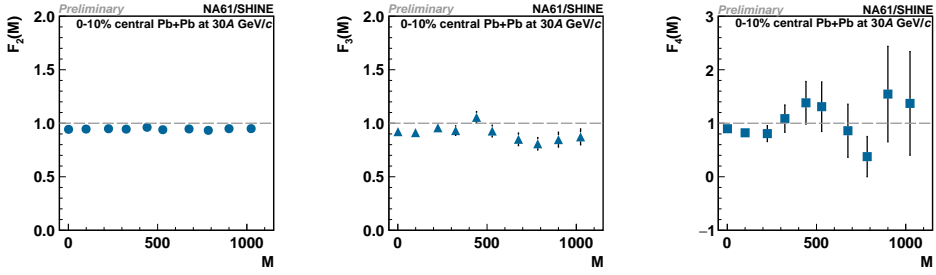


**Figure 6.** The dependence of the scaled factorial moments ( $F_2$ ,  $F_3$  and  $F_4$ ) of negatively charged particle multiplicity distribution on the number of subdivisions in cumulative transverse-momentum space  $M$  for  $1 \leq M \leq 32^2$  for central (0-10%)  $^{208}\text{Pb} + \text{Pb}$  at 30A GeV/c collisions. The results for  $F_2$ ,  $F_3$  and  $F_4$  are plotted from *left to right*. Only statistical uncertainties are indicated.

## 6 Summary

This proceeding reports on the ongoing NA61/SHINE search for the critical point of the strongly interacting matter. The results for central  $^{208}\text{Pb} + \text{Pb}$  collision at 13A GeV/c, 30A GeV/c and  $^{40}\text{Ar} + ^{45}\text{Sc}$  collisions at 13A-150A GeV/c are presented. The scaled factorial moments of proton and negatively charged hadron multiplicity distribution at mid-rapidity are shown as a function of the number of subdivisions in the cumulative transverse-momentum components. Independent data sets were used to calculate results for each subdivision. The results show no indication of the intermittency signal. The intermittency analysis of other reactions recorded within the NA61/SHINE program on strong interactions is well advanced, and new results should be expected soon.

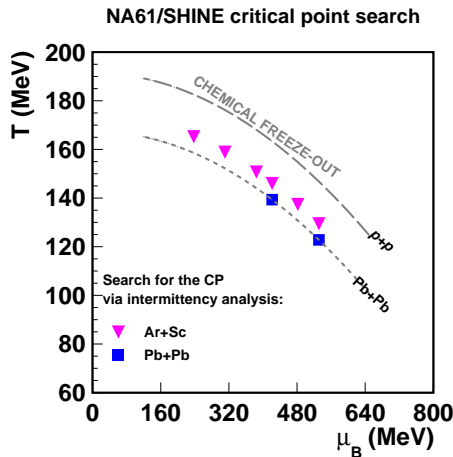


**Figure 7.** Diagram of chemical freeze-out temperature and chemical potential. The dashed line indicates parameters in  $p+p$  interactions and the dotted line in central Pb+Pb collisions [25]. The colored points mark reactions in the  $T - \mu_B$  phase diagram for which search for the critical point was conducted.

## 7 Acknowledgements

This work is supported by the National Science Centre, Poland under grant no. 2018/30/A/ST2/0026.

## References

- [1] N. Abgrall et al. (NA61/SHINE), JINST **9**, P06005 (2014), 1401.4699
- [2] A. Aduszkiewicz (NA61/SHINE), Tech. Rep. CERN-SPSC-2018-029. SPSC-SR-239, CERN, Geneva (2018), <https://cds.cern.ch/record/2642286>
- [3] J. Wosiek, Acta Phys. Polon. **B19**, 863 (1988)
- [4] A. Bialas, R.B. Peschanski, Nucl. Phys. **B273**, 703 (1986)
- [5] H. Satz, Nucl.Phys. **B326**, 613 (1989)
- [6] N.G. Antoniou, E.N. Argyres, C.G. Papadopoulos, A.P. Contogouris, S.D.P. Vlassopoulos, Phys. Lett. **B245**, 619 (1990)
- [7] A. Bialas, R. Hwa, Phys.Lett. **B253**, 436 (1991)
- [8] T. Anticic et al. (NA49), Eur. Phys. J. C **75**, 587 (2015), 1208.5292
- [9] M.A. Stephanov, K. Rajagopal, E.V. Shuryak, Phys. Rev. Lett. **81**, 4816 (1998), hep-ph/9806219
- [10] M.A. Stephanov, K. Rajagopal, E.V. Shuryak, Phys.Rev. **D60**, 114028 (1999), hep-ph/9903292
- [11] N.G. Antoniou, F.K. Diakonov, A.S. Kapoyannis, K.S. Kousouris, Phys. Rev. Lett. **97**, 032002 (2006), hep-ph/0602051
- [12] N. Antoniou, Y. Contoyiannis, F. Diakonov, A. Karanikas, C. Ktorides, Nucl.Phys. **A693**, 799 (2001), hep-ph/0012164
- [13] M.A. Stephanov, Prog. Theor. Phys. Suppl. **153**, 139 (2004), [Int. J. Mod. Phys.A20,4387(2005)], hep-ph/0402115
- [14] K. Fukushima, T. Hatsuda, Rept. Prog. Phys. **74**, 014001 (2011), 1005.4814
- [15] Y. Hatta, T. Ikeda, Phys.Rev. **D67**, 014028 (2003), hep-ph/0210284
- [16] N. Antoniou, F. Diakonov, A. Kapoyannis, Phys.Rev. **C81**, 011901 (2010), 0809.0685
- [17] F. Karsch, K. Redlich, Phys. Lett. **B695**, 136 (2011), 1007.2581
- [18] V. Skokov, B. Friman, K. Redlich, Phys. Rev. **C83**, 054904 (2011), 1008.4570
- [19] K. Morita, V. Skokov, B. Friman, K. Redlich, Eur. Phys. J. **C74**, 2706 (2014), 1211.4703
- [20] Y. Hatta, M.A. Stephanov, Phys. Rev. Lett. **91**, 102003 (2003), [Erratum: Phys. Rev. Lett.91,129901(2003)], hep-ph/0302002
- [21] A. Bialas, M. Gazdzicki, Phys. Lett. B **252**, 483 (1990)
- [22] S. Samanta, T. Czopowicz, M. Gazdzicki, Nucl. Phys. A **1015**, 122299 (2021), 2105.00344
- [23] NA61/SHINE acceptance map available at <https://edms.cern.ch/document/2778197>
- [24] T. Czopowicz (NA61/SHINE), PoS **CPOD2021**, 039 (2021)
- [25] F. Becattini, J. Manninen, M. Gazdzicki, Phys.Rev. **C73**, 044905 (2006), hep-ph/0511092